Controlling the reproducibility of Coulomb blockade phenomena for gold nanoparticles on an organic monolayer/silicon system

L Caillard, S Sattayaporn, A-F Lamic-Humblot, S Casale, P Campbell, y J Chabal, Olivier Pluchery

Controlling the reproducibility of Coulomb blockade phenomena for gold nanoparticles on an organic monolayer/silicon system

L. Caillard[1,2], S. Sattayaporn[1], A-F. Lamic-Humblot[3], S. Casale[3], P. Campbell[2], Y. J. Chabal[2], O. Pluchery[1]

[1] Sorbonne Universités, UPMC Univ Paris 06, UMR CNRS 7588, Institut des NanoSciences de Paris, 4 place Jussieu, F-75005 Paris, France,

[2] Laboratory for Surface and Nanostructure Modifications, Department of Materials Science and Engineering, University of Texas at Dallas, 800 West Campbell Road, Dallas, Texas 7508, USA,

[3] Sorbonne Universités, UPMC Univ Paris 06, UMR CNRS 7197, Laboratoire de Réactivité de Surface, 4 place Jussieu, case 178, F-75005 Paris, France.

Corresponding author: olivier.pluchery@insp.jussieu.fr

Abstract. Two types of highly ordered organic layers were prepared on silicon modified with an amine termination for binding gold nanoparticles (AuNPs). These two Grafted Organic Monolayers (GOMs), consisting of alkyl chains with seven or eleven carbon atoms, were grafted on oxide-free Si(111) surfaces as tunnel barriers between the silicon electrode and the AuNPs. Three kinds of colloidal AuNPs were prepared by reducing $HAuCl_4$ with three different reactants: citrate (Turkevich synthesis, diameter ~16 nm), ascorbic acid (diameter ~ 9 nm) or $NaBH_4$ (Natan synthesis, diameter ~7 nm). Scanning tunnel spectroscopy (STS) was performed in a UHV STM at 40K, and Coulomb blockade behaviour observed. The reproducibility of the Coulomb behaviour was analysed as a function of several chemical and physical parameters: size, crystallinity of the AuNPs, influence of surrounding surfactant molecules, and quality of the GOM/Si interface (degree of oxidation after the full processing). Samples were characterized with STM, STS, AFM, FTIR, XPS and HR-TEM. We show that the reproducibility in observing Coulomb behaviour can be as high as ~ 80% with the Natan synthesis of AuNPs and GOMs with short alkyl chains.

1

1. Introduction

In the design of new architectures and new devices for nanoelectronics, the question of reproducibility is often a major concern. When single charge electronics is targeted, the challenge is even more serious, since the core of the device is a metallic nanoparticle or a quantum dot, that needs to be positioned with an accuracy better than 0.1 nm to form a reproducible tunnel barrier junction with the source electrode.[1] Single charge electronics have received a strong interest in the early 2000s[2-4] and more recently the successful operation of a variety of devices was demonstrated such as single charge transistors,[5-8] organic-memory transistors,[9] metal-organic insulator-semiconductor solar cells,[10] floating-gate memories[11]. These prototype devices open the route to a built-in logical electronics where the discrete nature of the current is used to directly implement logical functions.[12-15] Nevertheless, one operational device is usually obtained at the cost of discarding many others. For example, in the case of the single electron transistor described by Koh and coworkers, the yield for fabricating operational devices was about 1%.[6] State of the art lithography was used in this case, and the issue is not in the fabrication process but the hot question is to delineate the possible origins for lack of reproducibility.

In the present study, we investigate the possibility of using hybrid interfaces made of highly ordered molecular layers on semiconductor surfaces for single charge electronics. We prepared a double barrier tunnel junction (DBTJ) where one junction is formed by a Grafted Organic Monolayer (GOM) situated between a gold nanoparticle (AuNP) and a silicon substrate, and the second junction is formed by the gap between the AuNP and the tip of a scanning tunneling microscope (STM) as depicted in **Figure 1**a. We present a detailed study of key parameters that are relevant to obtain reproducible Coulomb blockade behaviors, such as the nanoparticle size, shape and crystallinity, as well as the quality of the GOM and the effect of aging of the silicon substrate (local oxidation).

Coulomb blockade is observed when electrons are allowed to go through an *island* (a metallic or semiconductor nanoparticle) one by one. The particle must be at the nanometer scale in order to observe Coulomb blockade at room temperature[16, 17] except for very special designs.[18] In a practical way, single electron phenomena are detected as a stepwise increase of the current going through the island, upon increase of the applied potential as shown in **Figure 1**c. In the literature and to the best of our knowledge, two studies describe single charge architectures where one of the electrodes is a semiconductor substrate: Radojkovic *et al.* reported in 1996 Coulomb staircase *I-V* curves for 3 nm gold aggregates drop-casted directly on silicon. Their results were frequency dependent and exhibits unexpected negative differential resistances. [19] Tedesco *et al.* acknowledged in 2010 the difficulty to observe reliable single electron transport and stress the importance of the depletion layer in the semiconductor.[20] Nevertheless using silicon substrate as an electrode is needed to move towards the compatibility with CMOS technology.

One of the challenges addressed in our study is therefore the use of a GOM as tunnel barrier layer on silicon. Ever since the discovery of atomically flat hydrogen-terminated silicon (111) surfaces in 1989[21] many chemical processes have been developed to replace the hydrogen atom by functional organic molecules, whether by using thermal activation,[22-25] UV activation,[25-28] electrochemical activation[29, 30] or chlorination.[25, 31, 32] These Si(111) surfaces, functionalized with a GOM, can remain oxide-free after for several days[33] or after several chemical post treatments aimed for example at grafting either gold nanoparticles[34] or quantum dots.[35] As a comparison, hydrogen-terminated (SiH) surfaces remain stable only a few minutes in typical ambient air (*i.e.* with some radicals, ozone, and low level corrosive gases), leading to levels of surface oxidation that are too high for electrical devices (*e.g.*, the efficiency of silicon solar cells[36] is severely degraded when $D_i > 10^{13}$ cm^{-2} eV^{-1}). The electrical properties of the resulting surfaces have been investigated in the context of electronic application[32, 37] and surfaces with very few defects can be achieved.[38-43] For example a density of interface states as low as $D_{it} = 2.10^{11}$ cm^{-2} eV^{-1} has been measured on n-doped Si(111) functionalized surfaces.[40] The quality of this GOM is critical for several reasons: it allows the stable attachment of a gold nanoparticle, it provides a protecting layer on top of the silicon in order to prevent the creation of electron traps due to oxidation, and it is used as an insulator with a controlled thickness between the

AuNP and the Si bulk. We have shown in our previous study that Coulomb staircases were observed with this hybrid structure and with an STM in UHV (base pressure 3×10^{-11} mbar) at low temperatures (30-40K). The shape of the I-V characteristic depends on the substrate doping and Coulomb blockade was observed for positive and negative bias. [42] However, the reproducibility of the single-electron transport measurements was rather poor. Coulomb blockade is highly sensitive to the actual morphology and electronic properties of the two tunnel junctions. **Figure 1**c shows a Scanning Tunnel Spectrum (STS) with clear Coulomb staircase features obtained on a 6.0 nm AuNP at 40K. However a nearby NP with the same morphological characteristics, probed a few minutes later, exhibit no Coulomb blockade even after several tries of data acquisitions (**Figure 1**d). Many reasons for this non predictable behavior can be proposed and they are schematically depicted on **Figure 1**b: (1) the size of the NP measured by STM might be slightly biased since STM topography is based on mapping the Local Density of States; (2) NP might not be spherical; (3) the fact that NP are mono or polycrystalline may also affect the electron transport; (4) the colloidal NP might still be surrounded by ligands which will influence the behavior of the tunnel junctions; (5) the GOM is made of small molecular domains and at the boundaries the electrical properties may fluctuate; (6) the STM tip is not perfectly stable and therefore the second junction also fluctuates; and finally (7) the passivation against substrate oxidation carried out by the GOM is limited in time and local electrical defects progressively arise. Unfortunately, there is no easy experimental setup that allows measuring simultaneously an STS curve and probing the parameters listed above. Therefore in this study, we will draw our conclusions on a basis of a statistical approach comparing the amount of STS that exhibit Coulomb blockade to the other parameters.

Figure 1: *Sketch of the Double Barrier Tunnel Junction (DBTJ) used in the present work for measuring Coulomb blockade in the ideal case (a) and in the real experiments (b) where many imperfections may affect the STS measures: (1) inaccurate NP size, (2) non-spherical shape, (3) polycrystalline particles, (4) remains of molecular ligands, (5) molecular domains boundaries (6) tip instabilities and (7) local substrate oxidation. On a same sample, two close-by nanoparticles may exhibit clear Coulomb blockade I-V curves (c) or nothing detectable like in graph (d).*

2. Experimental

2.1. Sample preparation

2.1.1. Surface preparation

Functionalization of atomically flat, H-terminated Si surfaces has been described previously.[23, 42] Briefly, a 500 micron-thick Si(111) sample is cut into 15x38mm rectangle from a n-doped silicon wafer (polished on both sides). The resistivity of the substrate was 0.02 Ω.cm (carrier density of 1×10^{18} cm^{-3}) for all experiments, except for performing FTIR characterization in transmission where low doped substrates were used with a resistivity of 1-10 Ω.cm (carrier density of 1×10^{18} cm^{-3}). The sample is cleaned in a piranha solution ($H_2SO_4+H_2O_2$ 3:2) for 15min at 80°C. The native oxide layer is then stripped using a diluted HF (10%) solution for 30sec. The H-terminated surface is etched in a NH_4F (40%) solution for 2min30 at room temperature to get an atomically flat surface.[35] The oxide-free monohydride-terminated sample is then immersed in a neat solution of 10-carboxydecyl (SiC_{11}, long carbon chain) or in a neat solution of 6-carboxydecyl (SiC_7, short carbon chain). The SiC_{11} grafting is done in a heated solution (200°C), which has been degassed (oxygen free) through three successive freezing-pump-thaw cycles using liquid nitrogen. The reaction lasts for 4 hours. The SiC_7 grafting is done using UV activation in a customized quartz cell where the sample is sandwiched between two quartz slides. All the manipulations are carried out in a nitrogen-purged glove box (UNIlab Glovebox Workstation MBRAUN) with a O_2 and H_2O level lower than 0.1 ppm. It is then irradiated (with 253, 350 and 375 nm wavelengths) for 4h. UV activation is used for the SiC_7 molecules to reduce the amount of chemical needed: thermal hydrosilylation requires a higher amount of molecules and would require SiC_7 molecules to be diluted in mesitylene. The latter has a boiling point of 164.7°C, requiring a reaction temperature lower than the preferred 200°C and leading to a lower quality surface.

After the reaction, both samples are rinsed in boiling dichloromethane (40°C). Amine-terminated surfaces are obtained by deprotection for 1min30 in a potassium-tert-butoxide solution using dimethyl sulfoxide (DMSO) as solvent, and activation for 1min in N-ethyl-N'-(3-(dimethylamino)propyl)-carbodiimide (EDC) before adding ethylenediamine to the solution and keeping it at room temperature for 1h30. The resulting surfaces exhibit an amine group on top of the layer as shown in the inset of Fig. 1-a.[39, 41, 44] The samples are then characterized with X-ray photoelectron spectroscopy (XPS) and Fourier transform infrared spectroscopy (FTIR) measurements in order to assess their quality.

2.1.2. Gold nanoparticle preparation

Gold nanoparticles can then be chemically attached on the amine head groups. Three different synthesis methods have been used to prepare the AuNPs. All the chemicals were purchased from Sigma-Aldrich.

Turkevich method: The citrate reduction method for synthesizing gold nanoparticles in water was pioneered by Turkevich *et al.* in 1951[45] and modified by Frens in 1973.[46] As of today it is one of the most popular methods to synthesize spherical monodisperse gold nanoparticles.[47] An aqueous solution of $HAuCl_4$ (20 mL, 0.25 mM) is heated up at 100°C with vigorous stirring. Tri-sodium citrate is quickly added (1 mL, 18 mM), resulting in a change of color from yellow to purple within 4−5 min. In this reaction, citrate is first used as a reducing agent but also tends to adsorb onto the metallic gold clusters. It results in a size regulation of the obtained nanoparticle because the process is slowed down. Moreover, citrate ions are negatively charged such that the nanoparticles repel each other.[48, 49]

Ascorbic acid method: The method used to synthesize nanoparticles with ascorbic acid is described elsewhere.[47, 50] Typically, 200 µL of an aqueous solution of $HAuCl_4:3H_2O$ (10 g L^{-1} of gold) is added to 25 mL of water at around 0°C (ice-cooled) in a beaker. Then, 1.5 mL of a Na_2CO_3 solution

(21.2 g L^{-1}) and 1 mL of an ascorbic acid solution (7 g L^{-1}) are added under vigorous stirring. The solution becomes instantaneously dark red.

Natan method: This synthesis is based on the work of Natan *et al*.[51] then modified by Dong *et al*.[52] It is a modified version of the previously described Turkevich method. 2ml of $HAuCl_4$ (aq) 1% are added to 2ml of sodium citrate (aq) 1% in 100ml of water at 0°C. 1,5ml of a 0.075% solution of $NaBH_4$ is then added, resulting in a spontaneous color change to dark red.

2.1.3. Attachment of gold nanoparticles

Both Turkevich method and Natan method deposition are performed by simply dipping the functionalized surfaces in the colloidal solutions. Turkevich AuNPs are deposited during a 30 min dipping time whereas 1 min only is needed with the Natan technique. The ascorbic acid gold nanoparticle deposition requires that the pH of the solution is lowered down to 6 (use a 0.1 M hydrochloric acid solution) before dipping. A deposition of 12 min is performed to obtain the desired surface coverage. Several rinsing with deionized water are carried out to remove the loose nanoparticles after each deposition. All samples are dried with a nitrogen stream. For each method, the attachment relies on the interaction between the $-NH_2$ moiety of the organic layer and the gold surface.

2.2. Characterization techniques

FTIR spectra are acquired using Nicolet 6700 FTIR spectrometer from Thermo Scientific equipped with a DTGS detector. Detection is performed in transmission at an angle of incidence of 74° with respect to the normal of the surface in a dry nitrogen-purged atmosphere. Highly doped silicon samples (resistivity lower than 1 Ω.cm) are not transparent in the mid-IR range (400-4000 cm^{-1}) and therefore it was not possible to characterize the doped samples used for Coulomb blockade with FTIR. This is why the FTIR characterization was carried out on a GOM prepared on low doped silicon substrates. Hydrosilylation can be carried out identically whatever the doping provided special care is taken for keeping the amount of H_2O and O_2 in the glove box as low as possible, and avoid competitive oxidation.[27] In transmission, both sides are probed, thus increasing the signal, since both sides receive the same treatment during wet chemical functionalization.

Transmission electron microscope (TEM) images are collected with a JEOL JEM 2010 LaB6 microscope operating at 200 kV equipped with a charge-coupled device camera. Particle size measurements are performed with "ImageJ" (Image processing and analysis in Java, Open source). The limit of size detection is about 1 nm.

Scanning Tunneling microscopy (STM) is carried out with a commercial apparatus (Omicron VT- XA) in which the sample can be cooled down to 30-40 K with a cold finger in contact with liquid helium. The base pressure of the chamber is 3.10^{-11} mbar. The potential is applied to the sample relative to the tip. After acquiring an STM image, current-voltage spectra *I-V* are recorded with scanning tunneling spectroscopy (STS) on various AuNPs having separation from neighboring particles of at least one nanoparticle diameter. The tip is placed above a given AuNP at a distance determined by the current set point used for imaging (typical values for imaging are from 20 to 50 pA). A temperature of 40 K is obtained with a constant He flow that leads to a lateral drift of roughly 0.4 nm/min after 1h stabilization time. For each image and before I-V acquisition, this drift is precisely calculated, and a correction is applied so that the tip does not move more than 0.01 nm over a nanoparticle during data acquisition. Series of 10 sweeps are then acquired for each measurement. Several measurements are done on each AuNP. Each curve however is treated individually since the tip can move or vibrate during a sweep, which sometimes alters the *I-V* curve.

3. Results

The approach adopted in the present study is based on statistics in order to draw some general conclusions on the effects from the parameters listed in the following.

3.1. Nanoparticle size and shape

From TEM images we obtained a size distribution of each colloidal solution, as illustrated in **Figure 2**. Accordingly to the literature[47, 53] the Turkevich method provided particles with a narrow size distribution and a diameter that can be adjusted at values above 12 nm by changing the ratio of citrate over $HAuCl_4$. A ratio [citrate]/[$HAuCl_4$] = 3 very reproducibly provided 16.6 nm AuNPs as measured for solution #5 in Table 1. Smaller particles were achieved with the ascorbic acid method (8.5 nm) but with a wider standard deviation (2.4 nm). This standard deviation was narrowed down to 1.3 nm by using $NaBH_4$ as reducing agent and citrate as surfactant. This is the Natan method that leads to the production of NPs of intermediate size (6.6 nm). NP size was also cross-checked with AFM (see SI) and STM. With these scanning probe microscopy images, the main purpose was to assess the NP surface coverage after deposition on the functionalized substrate. Size was measured as the height of the protrusions and not as the apparent lateral size since this latter is amplified due to the convolution with the AFM or STM tip. Typical lateral sizes were 20 nm with AFM and 15 nm with STM for a 8 nm nanoparticle. The size measured with all three methods provided compatible values given the size distributions obtained by the different techniques (See Table 1). From Table 1, STM seems to measure particles smaller of 1.0 to 1.5 nm. For example with solution #1, the same sample, when analyzed with AFM exhibit particles of height 9.6 ±1.9 nm and 8.1±2.1 nm with STM. There is no technical reason for a systematic size deviation with STM, even if topography is measured indirectly with STM. The variation of the typical tip-sample distance due to scanning over different material (NP to GOM) will not exceed 0.5 nm and we cannot expect size deviation larger than this value. However with STM, our aim was to detect Coulomb blockade and we intentionally searched for smaller particles therefore this deviation was due to non-random sampling. In the following, we will consider that the size measured with STM corresponds to the actual diameter of the AuNPs.

Regarding the NP shape, the most regular NP (spherical) were the Turkevich ones with just 4% of them displaying an aspect-ratio greater than 1.25. The aspect ratio of an ellipsoid is the ratio of the long axis over the short axis of the ellipse. Ascorbic AuNPs tended to produce more non-spherical NP with 26% displaying an aspect-ratio greater than 1.25. On the other hand, Natan method produced just 8% of elliptic AuNPs. Therefore, since Turkevich AuNPs are too large for observing room temperature Coulomb blockade, Natan's method seems to be the best option to have spherical and reproducible nanoparticles.

NP type	HR-TEM				AFM	STM
	Size (nm)	% with A/R >1.25	% mono-crystalline	NP count	Size (nm)	Size (nm)
Asc - solution#1					9.6±1.9	8.1±2.1
Asc - solution#2	8.5±2.4	26%	31%	213		
Natan - solution#3	6.6±1.3	8%	47%	34	6.6±1.3	5.5±1.8
Turkevich - sol. #4					12.3±1.3	12.6±0.9
Turkevich - sol. #5	16.6±1.6	4%	0%	92	15.6±1.0	

Table 1: Size distribution (with standard deviation) of colloidal gold nanoparticles prepared by reduction of $HAuCl_4$ with three agents: ascorbic acid, $NaBH_4$ with citrate (Natan method) or citrate

(Turkevich method). The size of the nanoparticles is measured with TEM as well as the aspect ratio (A/R) and the proportion of monocrystalline particles. Their size is compared with the values obtained with AFM and STM after deposition on our surface.

3.2. Crystallinity of nanoparticles

High Resolution TEM allows the identification of the crystalline character of the NPs. For monocrystalline particles, parallel atomic planes are visible in the high resolution images (HR-TEM images given in the SI). When the particles are polycrystalline, two or more families of planes are identified. However sometimes, the electron beam is off-axis relative to all possible crystallographic planes and the particle looks amorphous although it might be a misaligned monocrystalline one. In this case, when it was not possible to determine the crystallinity of some particles they are labeled as "undefined" (between 11% and 23% of all the analyzed particles for each method). As shown in **Figure 2**-c, Turkevich method produced polycrystalline NP exclusively. The preparation method with ascorbic acid produced 31% of monocrystalline particles and Natan synthesis, 47%.

The detailed analysis is summarized in the three histograms of **Figure 2**-d where the size distribution is indicated as well as the mono- or poly crystalline proportion for each class of sizes. Notice that the undefined NPs have been discarded in the histograms. This accurate balance between mono- and poly-crystalline particles as a function of their size is important in order to assess what is the proportion of monocrystalline particles probed with STS.
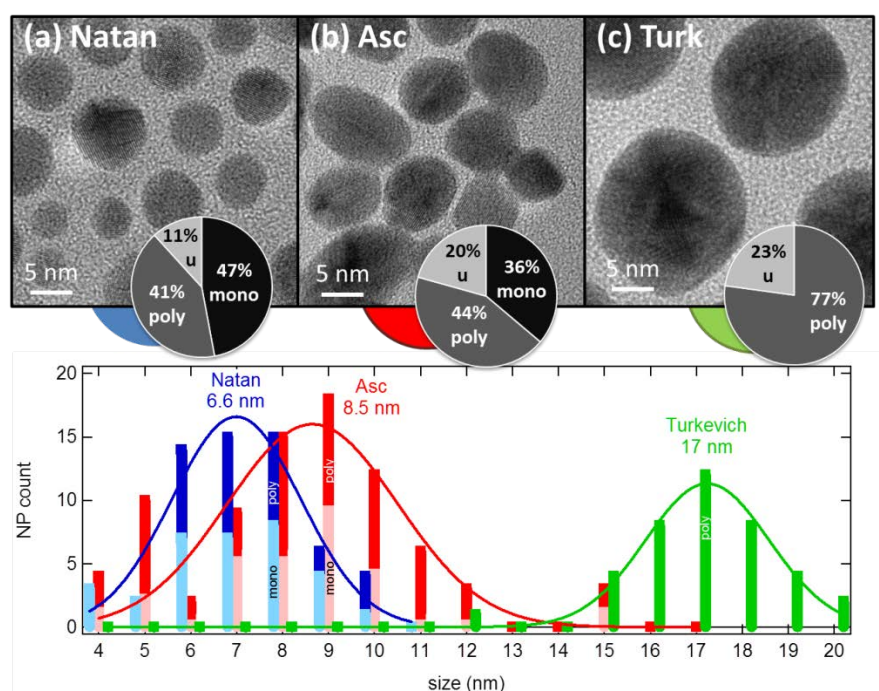

Figure 2: *TEM images of gold nanoparticles synthesized with Natan method (a, Natan, blue), ascorbic acid method (b, Asc, red) and Turkevich method (c, Turk, green) with the size distribution for each method. The insets indicate the proportion of monocrystalline (black, mono), polycrystalline (dark grey, poly) and undefined nanoparticles (light grey, u) for each synthesis method. The histograms show the size distribution of the three kinds of nanoparticles including the balance between mono and polycrystalline nanoparticles for each class of size.*

3.3. Nanoparticle coverage

The nanoparticle coverage after deposition is evaluated with AFM as detailed in the Supplemental Info. A coverage of 3.4×10^{10} NP.cm^{-2} was achieved for Natan NP and of 7×10^9 NP.cm^{-2} with ascorbic NP.

3.4. Removal of the ligands by annealing

One origin of STS measurement instabilities might be the presence of ligands around the metallic nanoparticles. Ligands are organic molecules that prevent nanoparticles from sintering when they are in the aqueous solution. However, they act as electric insulators with sometimes hardly predictable properties and this is why their removal is important once the nanoparticles are deposited. We investigate the effect of a low-temperature (100 to 250°C) and short time annealing in ultra-high vacuum on various samples as a way for removing the organic stabilizing layer.

Regarding the effect on the deposited NP, they were checked with AFM before and after a 150°C vacuum annealing process. The size distribution was found to be similar, as the one shown in Table 1. In that case Ascorbic AuNPs were found to have an average diameter of 8.2+/-3.9 nm before annealing. The same sample was probed again with AFM after annealing and the average diameter was 9.6+/-4.4 nm (details in Supplemental Info). These results are in agreement with published results: the melting temperature of 5 nm AuNPs is known to be 800 °C which is well below the melting point of bulk gold (1064°C) but far above the temperatures we use.[54] Moreover no changes in the crystalline structure of the AuNPs were detected upon annealing at temperatures below 300°C as measured with *in situ* HR-TEM.[55] Finally since the nanoparticles are chemically grafted on the GOM, we can dismiss nanoparticle ripening, that would produce distinguishable aggregate that were never observed. Therefore we are confident that the mild annealing process at 150°C does not affect the nanoparticle structure and its attachment to the substrate. Moreover the three NP preparations we have selected for the present study are characterized by ligands with weak adsorption strength: the ligand is ascorbate for AuNPs prepared with ascorbic-acid and citrate for Turkevich and Natan techniques. Unlike thiol commonly used to stabilize gold nanoparticles, citrate and ascorbate are known for being replaced by other adsorbates in solution[56, 57] and are likely removed by annealing.

Regarding the effects of annealing on the GOM, the surface was first imaged using our UHV-STM at room temperature without any further treatment. Typical results showed instability of the surface and difficulty in obtaining a clean image: horizontal lines appeared in the images and they are characteristic of sudden changes in the tunneling current measurement (**Figure 3**a). This was caused by molecules physisorbed on the surface such as water molecules, ligands of the AuNP or molecules remaining from the deprotection and activation steps. These molecules tend to attach to the tungsten tip and create alternative current paths that resulted in highly unstable scans. Therefore annealing was a decisive step and three temperatures were tested for a fixed 30 min annealing time. As shown in **Figure 3** after a 250°C annealing, STM images showed that the surface was damaged (**Figure 3**c): dark areas with almost no AuNPs were detected in many parts of sample. The alkyl chains grafted on silicon are known to be stable up to 400°C[16.58] However, since these damaged areas exhibit a significant decrease in the number of gold nanoparticles, the degradation must be at the top part of the molecule where the amine group was located (see sketch in **Figure 1**-a). No single electron transport was observed on the few AuNPs present in these areas (only two AuNPs were encountered). **Figure 3**b shows a SiC$_{11}$ GOM with Turkevich AuNP after a 200°C annealing. The STM imaging was straightforward and homogenous proving that the surface was not damaged. The surface exhibits parallel lines due to the terraces of the silicon substrate. On the surface small area of *ca* 4 nm are also visible and are due to molecular domains formed by groups of molecules all tilted in the same direction (see **Figure 1**b) as discussed in our earlier study.[42] Therefore for all the other experiments, we carried out an annealing at 150-200°C for 30 min under UHV and it proved to be optimal for stable STS.
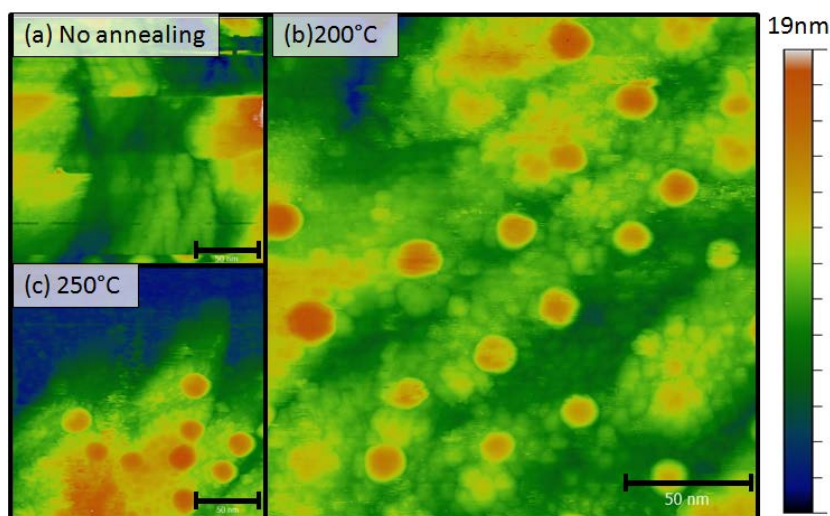
Figure 3: STM images of an activated SiC_{11} surface (i.e. amine-terminated monolayer) on silicon with gold nanoparticles deposited on top (using Turkevich technique). With no annealing (a), the surface is difficult to image due to a too high amount of physisorbed contaminants. With a 200°C annealing (b) imaging is optimal but following a 250°C annealing (c) dark areas start to appear on the surface that could be due to degradation of the organic layer. Scale bar: 50nm.

3.5. Quality of Si/GOM interface

It is well known that silicon quickly and spontaneously oxidizes.[59] For example the image of a clean Si(100)-2x1 is partially blurred after 5h STM imaging in a 10^{-10} mbar vacuum chamber, which corresponds to 5 sec stability in a 10^{-6} mbar vacuum chamber.[60, 61] Silicon passivation is a serious challenge. The SiC_7 and SiC_{11} surfaces studied in this work successfully take up this challenge and the influence of oxidation was studied as follows: some samples functionalized with SiC_7 were kept for two days in air. FTIR (see **Figure 4**) and XPS measurement (see Supplemental Info) reveal that oxidation is considerably slowed down as we already discussed in our previous study.[42] In **Figure 4**, we show transmission FTIR data for the SiC_7 GOM referenced to the oxide-free H-terminated Si(111) surface. The negative peak at 2083 cm^{-1} is due to the replacement of Si−H bonds with Si−C bonds during the UV hydrosilylation process. Comparison of the area of this peak with the positive one in the oxide-free Si(111) spectra (if referenced to the *oxidized* clean surface, not shown here) provides an estimate for hydrogen coverage of roughly ½ of the surface.[33] Half of the Si-H bonds were replaced by the active molecule in a homogeneous manner. The band at 1713 cm^{-1}, corresponds to the C=O bond of the ester (see **Figure 1**a for molecular model), the vibrations at 1280 and 1410 cm^{-1} correspond to the C-O bond, and 1461cm^{-1} is assigned to the bending mode of the methylene groups of the alkyl chain. The carbon chain is also identified by its 2855 and 2920 cm^{-1} stretch modes (CH_2). The black spectrum corresponds to a pristine sample and the red spectrum to the same sample after two days in air. The latter shows evidence for some oxidation with absorption bands at 1080 and 1240 cm^{-1} (TO and LO modes of SiO_2), which are negligible for the pristine one. The presence of a third carbon peak at 2988cm^{-1} (CH_3) suggests that there was some adventitious hydrocarbon at the surface as well. XPS analysis (see SI) confirms that oxidation starts being detectable after two days in air and allows estimating that 25% of the silicon surface atoms are oxidized.
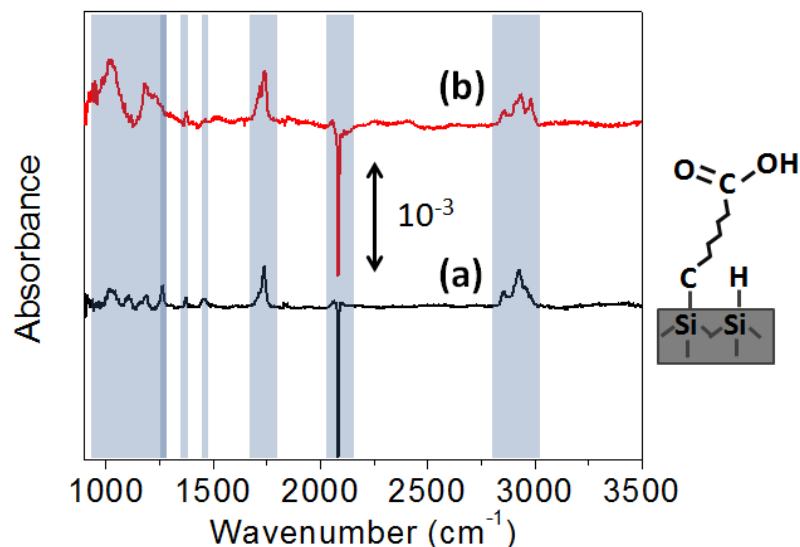
Figure 4: FTIR spectra of the functionalized surface after deprotection of the carboxylic acid for the SiC_7 molecule (a) and after two days in air (b). The sample that stayed in air shows signs of oxidation with the apparition of the TO an LO peaks at 1080 and 1240 cm^{-1} and some carbon contamination in the 3000 cm^{-1} region.

STM images of the oxidized sample show some dark areas that differ from those observed when over-annealing the sample. They appear "more noisy", an observation associated with oxidation. The insulating effect of the oxide makes the current less stable leading to this apparent "noise", and preventing a good imaging of the morphology. The images show that the oxidation is not homogeneous on the surface: it is a localized phenomenon, starting with a patch of silicon oxide that spreads with time.[62, 63] It is possible to encounter nanoparticles on these areas, but estimation of their size is inaccurate. Once again, no single-electron transport was ever observed on AuNPs on or next to these areas, indicating that a clean oxide-free surface is necessary for devices purposes. Nevertheless, a sample with some oxidized areas can still be used under UHV for single electron transport if NPs are selected *away* from these altered areas, *i.e.* measurements should only be performed on NPs grafted to oxide-free Si patches.[62]

4. Discussion

Observation of single electron transport has been optimally achieved using a short GOM (SiC_7), on oxide-free Si surfaces, with AuNPs synthesized with Natan method as shown in our previous study[42] (see also STS of **Figure 1**-c). However several reasons may prevent the single charge behavior of our DBTJ and we discuss the parameters that are causing this deviation from the ideal behavior. A nanoparticle will be considered "consistently active" in STS when it exhibits consistent single electron behavior: *i.e.* a characteristic Coulomb staircase behavior is observed for more than two third of the sweeps. In contrast, an AuNP will be considered "occasionally active" when it only displays single electron behavior on occasion, *i.e.* less than two third of the times. And it is "inactive" when Coulomb staircases are never observed. Several issues can account for this more erratic behavior as pictured in **Figure 1**-b and discussed below.

Size and shape of AuNP. In our experiments no Coulomb blockade was ever observed with Turkevich AuNPs even at 40K. This is not a surprise given their size larger than 12 nm (see Table 1). In principle Coulomb steps of 50-100 mV are expected with such NP sizes, but they are probably blurred because of thermal fluctuations and Coulomb staircase cannot be distinguished from the noise.

Therefore we focus on the two other preparation methods for smaller NPs. As summarized in Table 1 the AuNPs of interest are predominantly spherical; we will therefore not discuss the effect of non-spherical shapes.

Surfactant removal. In our experiments single electron transport has only been observed with oxide-free surfaces that went through a cleaning and ligand-removal process (30 min 150ºC annealing). The fact that no positive results were obtained without annealing can also be explained by the recent work of Xu *et al.*in 2009.[64] They have shown that ligands that surround a deposited nanoparticle widen the Coulomb blockade gap: increasing the concentration of surrounding molecules (hexane) shifts the first step to higher bias. For example, for a 6.3nm AuNP on a gold substrate, they shift the first step from 0.2V to 1.8V, which if applied to our asymmetrical structure (silicon substrate instead of gold) should displaced the first step to bias that we have not investigated (> 2 V). Therefore the annealing step proved to be critical. After this annealing step, positive results were obtained with the Natan and ascorbic AuNPs and with both linkers (SiC_7 and SiC_{11}) as shown in **Figure 5**. For example in **Figure 5**-a, two clear steps are measured with a 9 nm asc-AuNP. The other three graphs are obtained with smaller NPs of ~6 nm and exhibit three steps between 0 and 1.5 V. It is not the purpose of the present paper to discuss the dependence of the steps with NP size as it will be the subject of a specific study, including the effect of band bending in silicon. Regarding Coulomb blockade activity, the two kinds of AuNPs behave differently: on an Si-C7 surface, the activity is 64% for asc-AuNP and 82% for Natan-AuNP. Similar results are obtained with Si-C11 and are summarized in Table 2. This dissemblance of activity cannot be assigned to the nanoparticle size given that the size distributions of asc-AuNPs and Natan-AuNPs are very similar as shown in **Figure 2**.
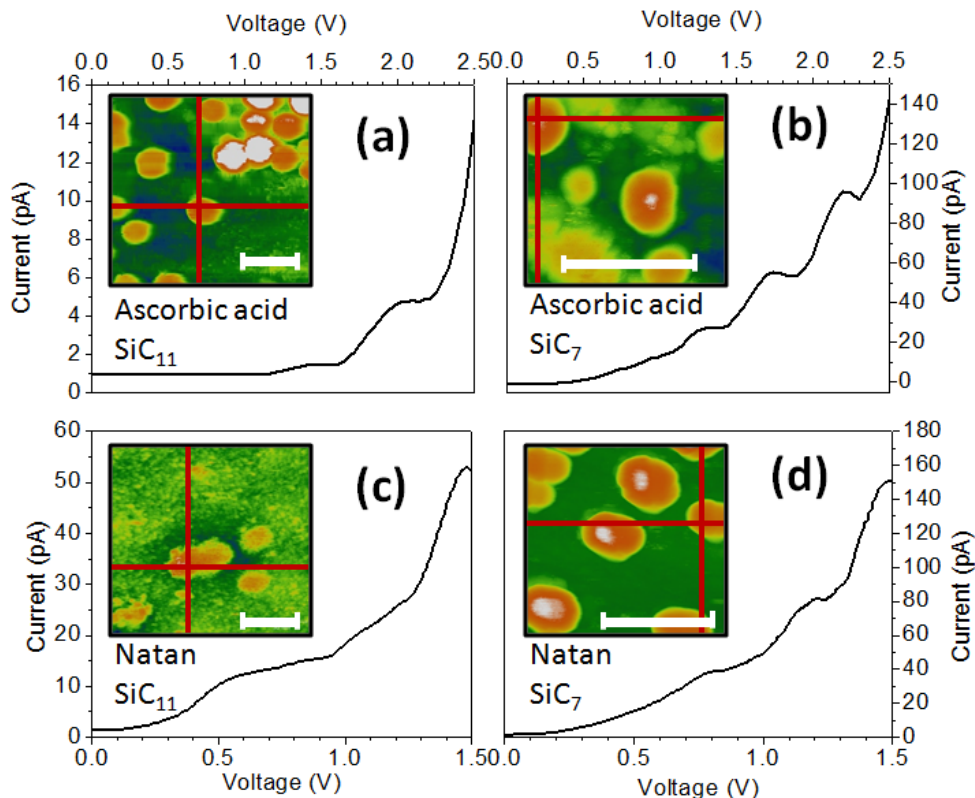

Figure 5: Examples of STS measurements performed on the different surfaces. Silicon surface functionalized with SiC_{11} molecule with an ascorbic acid AuNP of 9 nm grafted (a) and a Natan AuNP of 6 nm grafted (c). Silicon surfaces functionalized with SiC_7 molecule with an ascorbic acid AuNP of 6 nm grafted (b) and a Natan AuNP of 6.5 nm grafted (d). Each STS show staircase shape that is characteristic of single electron transport through coulomb staircase phenomena. An inset for each

curve shows an STM image of the investigated nanoparticle. All measurements are done at 30K. Scale bar: 50nm.

This is why we also question the influence of crystallinity on electron transport. **Figure 2** shows that 31% and 47% of AuNPs obtained with Ascorbic acid and Natan methods respectively, are single crystals. STS were acquired from a total of 64 nanoparticles. If we first focus our attention to the thinnest organic monolayer, SiC7, we measure that 64% of them were active for asc-AuNPs (12% occasionally and 52% consistently active) and that this activity rises to 82% with Natan-AuNPs (details in Table 2). But we cannot easily link the 31% mono-crystalline Asc-AuNPs to the 64% Coulomb activity. One reason is that with STS, we preferentially probed smaller particles (see Supplemental Info for details on the size distribution of NP probed with STS) and from **Figure 2**, we see that AuNPs are more likely monocrystalline when they are smaller. Therefore, for each AuNP probed in STS, we can compute the probability that this nanoparticle is monocrystalline, given its size and its preparation method. When we combine these results we end up with 47% of the Asc-AuNP probed in STS being monocrystalline and a reproducibility rate for Coulomb blockade of 59%. With Natan-AuNP, 70% are monocrystalline and the reproducibility is 73%. These data are presented in Table 2 and provide a strong trend: the reproducibility of Coulomb behavior is all the better, the NP are more mono-crystalline.

	Size (nm)	STS results on SiC$_{11}$		STS results on SiC$_7$		Active AuNP SiC$_{11}$ + SiC$_7$	% mono
		Occas + consist	NP count	Occas + consist	NP count		
Ascorbic acid	8.5±2.4	**8+41% = 51%**	12	**12+52% = 64%**	25	**59%**	**47%**
Natan	6.6±1.3	**9+45% = 54%**	11	**19+63% = 82%**	16	**70%**	**73%**
Turkevich	16.6±1.6	0%	18				

Table 2.summary of STS and HR-TEM results on the three different synthesis techniques.

Lu *et al.* reported in 2003 specific Coulomb blockade I-V curves on amorphous and monocrystalline palladium 2 nm NP at 4.2K.[65] They observe additional steps with monocrystalline NP compared to amorphous ones and they explain it with discrete resonant tunneling effect that is not visible with amorphous NP because of the shorter lifetime of electronic states. In our case, we cannot link one given STS to the crystalline nature of a particle. Moreover we work with larger nanoparticles with higher temperatures (40K and not 4.2K). Therefore a possible interpretation for higher reproducibility observed with monocrystalline AuNPs, is that the quality of the interface between the nanoparticle and the GOM is better when dealing with single crystals. It can be understood from **Figure 1** which is drawn on scale for a 6 nm AuNP. It shows that the attachment occurs through 4 or 5 molecules. For monocrystalline NPs, there is a higher probability that one crystallographic facet of a nanoparticle ensures a good bonding with these 4 or 5 molecules. In contrast, polycrystalline particles can offer multiple parallel current paths between the gold and the silicon bulk. Single electron transport can still be obtained with polycrystalline particles if the orientation with respect to the surface is optimum (*i.e.* one plane only), but the likelihood is lower than for single crystals.

The above results shown in **Figure 5** also point to the dependence on the thickness of the GOM. A thicker (*i.e.* SiC$_{11}$) monolayer appears to yield a lower amount of occasionally and consistently active AuNPs compared with thinner (*i.e.* SiC$_7$) monolayer. This is explained by the lower tunneling current through thicker organic layers, making it harder to detect single electron phenomena. The measured

current is lower and closer to the noise level of the electrical measurements. The current scale for STS measurements is hardly reproducible: it is highly dependent on parameters that are challenging to control such as drift, temperature, quality and shape of the tip. Typical current for an STS measurement on an AuNP (active or not) on SiC_7 has a value of 170 ± 100 pA for $V = 1.5$ V at a current setpoint 40 pA. On SiC_{11}, this value is 70 ± 40 pA. It shows that, even though the values fluctuate a lot, the typical current for the longer chain is several times lower. Step heights have been measured on a selection of active nanoparticles (both Natan and Ascorbic acid) which were investigated with the same current setpoint (40pA). Results give a step height of 30 ± 15 pA for NP on SiC_7 (total: 41curves) and 10 ± 7 pA for NP on SiC_{11} (total: 26 curves). This shows that, as expected, the typical step height for an active AuNP on SiC_7 is higher than on SiC_{11} even though the value can change a lot from one measurement to another. In the lower end of the step height values for AuNP on SiC_{11} we have current in the order of a few pA: it becomes comparable with the noise level of our STM (2-3pA), therefore the reliability of these value can be questionable and there may be lower scale steps that we couldn't accurately measure. Because of its higher current flux, SiC_7 is a better choice for single electron transport detection. However, one must consider that SiC_{11} GOM is a more stable surface (lifetime: 2 weeks in air) than SiC_7 GOM (lifetime: 2 days in air).

Finally, this analysis allows computing the average residence time of the electron in the AuNP for both organic layers. Electrons are flowing through the metallic island one by one (first step of the Coulomb staircase), at a given frequency. In the case of SiC_7, a step height of 30 pA yields an average residence time of an electron of $\tau = \frac{e}{\Delta i_{step}} = \frac{1.6 \times 10^{-19}}{30 \times 10^{-12}} = 5$ nsec. In the case of SiC_{11} $\Delta i_{step} = 11$ pA and this residence time is $\tau = 14$ nsec. If the goal were to fabricate single electron memories, the retention time is far too small. But this provides a starting point for designing thicker insulating layers and engineer single electron memories with reasonable storing times. In the present time, this organic layer appear well suited for designing a single electron transistor, where the current flow will be of the order of magnitude of 10 to 100 pA.

5. Conclusion

In this study we have shown that Grafted Organic Monolayers could serve as very efficient tunnel barrier on silicon Si(111) and form a Double Tunnel Barrier Junction with an STM tip. Reproducible Coulomb staircases are observed with two types of colloidal gold nanoparticles deposited on this organic layer: Asc-AuNP (8.5±2.4 nm) and Natan-AuNP (6.6±1.3 nm) provided they are cleaned from their organic surfactant with a mild UHV annealing at 150°C. Natan-AuNP provides a higher reproducibililty rate of 70% (59% for asc-AuNP) that we link to their higher single crystalline nature. An amount of silicon oxidation as low as ¼ of monolayer of oxygen is catastrophic for Coulomb behavior but the two types of GOM we describe are able to preserve the necessary quality of the surface for 2 or 3 days at room atmosphere.

After optimization of our architecture with respect to the described parameters, we observe single electron transport in 82% of the AuNP grafted on the SiC7 GOM. It proves that tailored highly ordered organic monolayers can be used for electrical functionalities with good reproducibility and it opens the way to special hybrid devices where silicon substrate and organic monolayers are used together.

Supplemental information
AFM images of AuNP deposited on our GOM, HR-TEM images of the three kinds of AuNP showing their crystalline structure, X-Ray Photoelecton spectra of the Si 2p peak and a histogram analysis of the sizes of AuNP probed with STM are provided in the Supplemental Information section, available via the Internet at http://iopscience.iop.org/0957-4484

References

1.   Cuevas, J. C.; Scheer, E., *Molecular Electronics*. World Scientific Publishing Company: London, 2010; p 724.
2.   Asahi, N.; Akazawa, M.; Amemiya, Y., Single-electron logic device based on the binary decision diagram. *Ieee Transactions on Electron Devices* **1997,** 44, (7), 1109-1116.
3.   Davidovic, D.; Tinkham, M., Coulomb blockade and discrete energy levels in Au nanoparticles. *Appl. Phys. Lett.* **1998,** 73, (26), 3959.
4.   Zabet-Khosousi, A.; Dhirani, A. A., Charge transport in nanoparticle assemblies. *Chem. Rev.* **2008,** 108, (10), 4072-4124.
5.   Yang, Y.; Nogami, M., Room temperature single electron transistor with two-dimensional array of Au-SiO2 core-shell nanoparticles. *Sci. & Techn. Adv. Mat.* **2005,** 6, (1), 71-75.
6.   Ray, V.; Subramanian, R.; Bhadrachalam, P.; Liang-Chieh Ma; Kim, C.-U.; Koh, S. J., CMOS-compatible fabrication of room temperature single-electron devices. *Nature Nanotechnology* **2008,** 3, 603-608.
7.   Khondaker, S. I.; Luo, K.; Yao, Z., The fabrication of single-electron transistors using dielectrophoretic trapping of individual gold nanoparticles. *Nanotechnology* **2010,** 21, (9), 095204.
8.   Tsai, L.-C.; Cheng, I.-C.; Tu, M.-C.; Chen, C.-D.; Lin, H.-Y., Formation of single-electron-transistors using self-assembly of nanoparticle chains. *Journal of Nanoparticle Research* **2010,** 12, (8), 2859-2864.
9.   Novembre, C.; Guerin, D.; Lmimouni, K.; Gamrat, C.; Vuillaume, D., Gold nanoparticle-pentacene memory transistors. *Appl. Phys. Lett.* **2008,** 92, (10).
10.   Har-Lavan, R.; Ron, I.; Thieblemont, F.; Cahen, D., Toward metal-organic insulator-semiconductor solar cells, based on molecular monolayer self-assembly on n-Si. *Appl. Phys. Lett.* **2009,** 94, (4), 043308 (3 pp.)-043308 (3 pp.).
11.   Chan, K. C.; Lee, P. F.; Dai, J. Y., Mesoscopic phenomena in Au nanocrystal floating gate memory structure. *Appl. Phys. Lett.* **2009,** 95, (11), 113109-3.
12.   Inokawa, H.; Fujiwara, A.; Takahashi, Y., A multiple-valued logic and memory with combined single-electron and metal-oxide-semiconductor transistors. *Electron Devices, IEEE Transactions on* **2003,** 50, (2), 462-470.
13.   Lientschnig, G.; Weymann, I.; Hadley, P., Simulating hybrid circuits of single-electron transistors and field-effect transistors. *Japanese Journal of Applied Physics Part 1-Regular Papers Short Notes & Review Papers* **2003,** 42, (10), 6467-6472.
14.   Likharev, K. K., Hybrid CMOS/Nanoelectronic Circuits: Opportunities and Challenges. *Journal of Nanoelectronics and Optoelectronics* **2008,** 3, (3), 203-230.
15.   Homberger, M.; Simon, U., On the application potential of gold nanoparticles in nanoelectronics and biomedicine. *Philos. T. Roy. Soc. A* **2010,** 368, (1915), 1405-1453.
16.   Likharev, K. K., Single-electron devices and their applications. *Proc. IEEE* **1999,** 87, (4), 606-632.
17.   Tekiel, A.; Miyahara, Y.; Topple, J. M.; Grutter, P., Room-Temperature Single-Electron Charging Detected by Electrostatic Force Microscopy. *ACS Nano* **2013,** 7, (5), 4683-4690.
18.   Bhadrachalam, P.; Subramanian, R.; Ray, V.; Ma, L.-C.; Wang, W.; Kim, J.; Cho, K.; Koh, S. J., Energy-filtered cold electron transport at room temperature. *Nat Commun* **2014,** 5, 4745.
19.   Radojkovic, P.; Schwartzkopff, M.; Enachescu, M.; Stefanov, E.; Hartmann, E.; Koch, F., Observation of Coulomb staircase and negative differential resistance at room temperature by

scanning tunneling microscopy. *J. Vac. Sci. Technol. B* **1996,** 14, (2), 1229-1233.

20.   Tedesco, J. L.; Rowe, J. E.; Nemanich, R. J., Titanium silicide islands on atomically clean Si(100): Identifying single electron tunneling effects. *Journal of Applied Physics* **2010,** 107, (12), 123715.

21.   Higashi, G. S.; Chabal, Y. J.; Trucks, G. W.; Raghavachari, K., Ideal hydrogen termination of the Si(111) surface. *Appl. Phys. Let.* **1990,** 56, (7), 656-8.

22.   Linford, M. R.; Fenter, P.; Eisenberger, P. M.; Chidsey, C. E. D., Alkyl Monolayers on Silicon Prepared from 1-Alkenes and Hydrogen-Terminated Silicon. *J. Am. Chem. Soc.* **1995,** 117, 3145-3155.

23.   Aureau, D.; Varin, Y.; Roodenko, K.; Seitz, O.; Pluchery, O.; Chabal, Y. J., Controlled deposition of gold nanoparticles on well-defined organic monolayer grafted on silicon. *J. Phys. Chem. C* **2010,** 114, (33), 14180–14186.

24.   Hacker, C. A., Modifying electronic properties at the silicon-molecule interface using atomic tethers. *Solid-State Electron.* **2010,** 54, (12), 1657-1664.

25.   Li, Y.; Calder, S.; Yaffe, O.; Cahen, D.; Haick, H.; Kronik, L.; Zuilhof, H., Hybrids of Organic Molecules and Flat, Oxide-Free Silicon: High-Density Monolayers, Electronic Properties, and Functionalization. *Langmuir* **2012,** 28, (26), 9920-9929.

26.   Voicu, R.; Boukherroub, R.; Bartzoka, V.; Ward, T.; Wojtyk, J. T. C.; Wayner, D. D. M., Formation, Characterization, and Chemistry of Undecanoic Acid-Terminated Silicon Surfaces: Patterning and Immobilization of DNA. *Langmuir* **2004,** 20, (26), 11713-11720.

27.   Miramond, C.; Vuillaume, D., 1-octadecene monolayers on Si(111) hydrogen-terminated surfaces: Effect of substrate doping. *J. Appl. Phys.* **2004,** 96, (3), 1529-1536.

28.   Faucheux, A.; Gouget-Laemmel, A. C.; Henry deVilleneuve, C.; Boukherroub, R.; Ozanam, F.; Allongue, P.; Chazalviel, J. N., Well-Defined Carboxyl-Terminated Alkyl Monolayers Grafted onto H-Si(111): Packing Density from a Combined AFM and Quantitative IR Study. *Langmuir* **2006,** 22, (1), 153-162.

29.   Teyssot, A.; Fidelis, A.; Fellah, S.; Ozanam, F.; Chazalviel, J. N., Anodic grafting of organic groups on the silicon surface. *Electrochimica Acta* **2002,** 47, (16), 2565-2571.

30.   Fellah, S.; Teyssot, A.; Ozanam, F. o.; Chazalviel, J.-N. l.; Vigneron, J.; Etcheberry, A., Kinetics of Electrochemical Derivatization of the Silicon Surface by Grignards. *Langmuir* **2002,** 18, (15), 5851-5860.

31.   Webb, L. J.; Rivillon, S.; Michalak, D. J.; Chabal, Y. J.; Lewis, N. S., Transmission Infrared Spectroscopy of Methyl- and Ethyl-Terminated Silicon(111) Surfaces. *J. Phys. Chem. B* **2006,** 110, (14), 7349-7356.

32.   Puniredd, S. R.; Assad, O.; Stelzner, T.; Christiansen, S.; Haick, H., Catalyst-Free Functionalization for Versatile Modification of Nonoxidized Silicon Structures. *Langmuir* **2011,** 27, (8), 4764-4771.

33.   Thissen, P.; Seitz, O.; Chabal, Y. J., Wet chemical surface functionalization of oxide-free silicon. *Progr. Surf. Sci.* **2012,** 87, (9-12), 272-290.

34.   Aureau, D.; Rappich, J.; Moraillon, A.; Allongue, P.; Ozanam, F.; Chazalviel, J.-N., In situ monitoring of the electronic properties and the pH stability of grafted Si(111). *The Journal of Electroanalytical Chemistry* **2010,** 646, (1-2), 33-42.

35.   Nguyen, H. M.; Seitz, O.; Aureau, D.; Sra, A.; Nijem, N.; Gartstein, Y. N.; Chabal, Y. J.; Malko, A. V., Spectroscopic evidence for nonradiative energy transfer between colloidal CdSe/ZnS nanocrystals and functionalized silicon substrates. *Appl. Phys. Let.* **2011,** 98, (16).

36.   Rahmouni, M.; Datta, A.; Chatterjee, P.; Damon-Lacoste, J.; Ballif, C.; Cabarrocas, P. R. I., Carrier transport and sensitivity issues in heterojunction with intrinsic thin layer solar cells on N-type crystalline silicon: A computer simulation study. *J. Appl. Phys.* **2010,** 107, (5).

37.   Vilan, A.; Yaffe, O.; Biller, A.; Salomon, A.; Kahn, A.; Cahen, D., Molecules on Si: Electronics with Chemistry. *Advanced Materials* **2010,** 22, (2), 140-159.

38.   Seitz, O.; Boecking, T.; Salomon, A.; Gooding, J. J.; Cahen, D., Importance of Monolayer Quality for Interpreting Current Transport through Organic Molecules: Alkyls on Oxide-Free Si.

Langmuir **2006,** 22, (16), 6915-6922.

39.   Seitz, O.; Fernandes, P. G.; Mahmud, G. A.; Wen, H.-C.; Stiegler, H. J.; Chapman, R. A.; Vogel, E. M.; Chabal, Y. J., One-Step Selective Chemistry for Silicon-on-Insulator Sensor Geometries. *Langmuir* **2011,** 27, (12), 7337-7340.

40.   Peng, W.; Seitz, O.; Chapman, R. A.; Vogel, E. M.; Chabal, Y. J., Probing the intrinsic electrical properties of thin organic layers/semiconductor interfaces using an atomic-layer-deposited Al2O3 protective layer. *Appl. Phys. Let.* **2012,** 101, (5), 051605-5.

41.   Seitz, O.; Caillard, L.; Nguyen, H. M.; Chiles, C.; Chabal, Y. J.; Malko, A. V., Optimizing non-radiative energy transfer in hybrid colloidal-nanocrystal/silicon structures by controlled nanopillar architectures for future photovoltaic cells. *Appl. Phys. Let.* **2012,** 100, (2), 021902.

42.   Caillard, L.; Seitz, O.; Campbell, P.; Doherty, R.; Lamic-Humblot, A.-F.; Lacaze, E.; Chabal, Y. J.; Pluchery, O., Gold nanoparticles on oxide-free silicon-molecule interface for single electron phenomena. *Langmuir* **2013,** 29, (16), 5066–5073.

43.   Nimmo, M. T.; Caillard, L. M.; De Benedetti, W.; Nguyen, H. M.; Seitz, O.; Gartstein, Y. N.; Chabal, Y. J.; Malko, A. V., Visible to Near-Infrared Sensitization of Silicon Substrates via Energy Transfer from Proximal Nanocrystals: Further Insights for Hybrid Photovoltaics. *Acs Nano* **2013,** 7, (4), 3236-3245.

44.   Seitz, O.; Dai, M.; Aguirre-Tostado, F. S.; Wallace, R. M.; Chabal, Y. J., Copper-Metal Deposition on Self Assembled Monolayer for Making Top Contacts in Molecular Electronic Devices. *J. Am. Chem. Soc.* **2009,** 131, (50), 18159-18167.

45.   Turkevich, J.; Stevenson, P. C.; Hillier, J., A study of the nucleation and growth processes in the synthesis of colloidal gold. *Discuss. Faraday Soc.* **1951,** 11, 55-75.

46.   Frens, G., Controlled Nucleation for Regulation of Particle-Size in Monodisperse Gold Suspensions. *Nature-Physical Science* **1973,** 241, (105), 20-22.

47.   Kimling, J.; Maier, M.; Okenve, B.; Kotaidis, V.; Ballot, H.; Plech, A., Turkevich Method for Gold Nanoparticle Synthesis Revisited. *J. Phys. Chem. B* **2006,** 110, (32), 15700-15707.

48.   Roucoux, A.; Schulz, J.; Patin, H., Reduced transition metal colloids: A novel family of reusable catalysts? *Chem. Rev.* **2002,** 102, (10), 3757-3778.

49.   Ji, X. H.; Song, X. N.; Li, J.; Bai, Y. B.; Yang, W. S.; Peng, X. G., Size control of gold nanocrystals in citrate reduction: The third role of citrate. *J. Am. Chem. Soc.* **2007,** 129, 13939-13948.

50.   Stathis, E. C.; Fabrikanos, A., Preparation of Colloidal Gold. *Chem. Ind.* **1958**, (27), 860-861.

51.   Grabar, K. C.; Allison, K. J.; Baker, B. E.; Bright, R. M.; Brown, K. R.; Freeman, R. G.; Fox, A. P.; Keating, C. D.; Musick, M. D.; Natan, M. J., Two-dimensional arrays of colloidal gold particles: A flexible approach to macroscopic metal surfaces. *Langmuir* **1996,** 12, (10), 2353-2361.

52.   Qu, X. H.; Peng, Z. Q.; Jiang, X.; Dong, S. J., Surface charge influence on the surface plasmon absorbance of electroactive thiol-protected gold nanoparticles. *Langmuir* **2004,** 20, (7), 2519-2522.

53.   Diegoli, S.; Mendes, P. M.; Baguley, E. R.; Leigh, S. J.; Iqbal, P.; Diaz, Y. R. G.; Begum, S.; Critchley, K.; Hammonds, G. D.; Evans, S. D.; Attwood, D.; Jones, I. P.; Preece, J. A., PH-dependent gold nanoparticle self-organization on functionalized Si/SiO2 surfaces. *J. Exper. Nanoscience* **2006,** 1, (3), 333-353.

54.   Buffat, P.; Borel, J. P., Size Effect on Melting Temperature of Gold Particles. *Phys. Rev. A* **1976,** 13, (6), 2287-2298.

55.   Young, N. P.; van Huis, M. A.; Zandbergen, H. W.; Xu, H.; Kirkland, A. I., Transformations of gold nanoparticles investigated using variable temperature high-resolution transmission electron microscopy. *Ultramicroscopy* **2010,** 110, (5), 506-516.

56.   Viudez, A. J.; Madueno, R.; Pineda, T.; Blazquez, M., Stabilization of gold nanoparticles by 6-mercaptopurine monolayers. Effects of the solvent properties. *J. Phys. Chem. B* **2006,** 110, (36), 17840-17847.

57.   Basu, S.; Ghosh, S. K.; Kundu, S.; Panigrahi, S.; Praharaj, S.; Pande, S.; Jana, S.; Pal, T., Biomolecule induced nanoparticle aggregation: Effect of particle size on interparticle coupling. *J. Colloid & Interf. Sci.* **2007,** 313, (2), 724-734.

58.   Jaeckel, B.; Hunger, R.; Webb, L. J.; Jaegermann, W.; Lewis, N. S., High-Resolution Synchrotron Photoemission Studies of the Electronic Structure and Thermal Stability of CH3- and C2H5-Functionalized Si(111) Surfaces. *The Journal of Physical Chemistry C* **2007,** 111, (49), 18204-18213.

59.   Cahill, D. G.; Avouris, P., Si Ejection and Regrowth During the Initial-Stages of Si(001) Oxidation. *Appl. Phys. Let.* **1992,** 60, (3), 326-328.

60.   Pluchery, O.; Coustel, R.; Witkowski, N.; Borensztein, Y., Adsorption of phenylacetylene on Si(100)-2 x 1: Kinetics and structure of the adlayer. *J. Phys. Chem. B* **2006,** 110, 22635-22643.

61.   Herzog, F.; Finocchi, F.; Soukiassian, L.; Pluchery, O., The adsorption of a substituted benzene, the ethynyl-trifluorotoluene on Si(100)-2x1. *Surface Science* **2011,** 605, (1-2), 166-173

62.   Fadjie-Djomkam, A. B.; Ababou-Girard, S.; Godet, C., Barrier height distribution and dipolar relaxation in metal-insulator-semiconductor junctions with molecular insulator: Ageing effects. *J. Appl. Phys.* **2012,** 112, (11), 113701-11.

63.   Zhang, Y.; Pluchery, O.; Caillard, L.; Lamic-Humblot, A.-F.; Casale, S.; Chabal, Y. J.; Salmeron, M., Sensing the Charge State of Single Gold Nanoparticles via Work Function Measurements. *Nano Letters* **accepted**.

64.   Xu, L.-P.; Chen, S., Scanning tunneling spectroscopy of gold nanoparticles: Influences of volatile organic vapors and particle core dimensions. *Chem. Phys. Lett.* **2009,** 468, (4-6), 222-226.

65.   Lu, W.; Wang, B.; Wang, K. D.; Wang, X. P.; Hou, J. G., Synthesis and characterization of crystalline and amorphous palladium nanoparticles. *Langmuir* **2003,** 19, (14), 5887-5891.